Nongray Gas Analyses for Reflecting Walls Utilizing a Flux Technique

J. A. Menart
Department of Mechanical Engineering,
University of Minnesota,
Minneapolis, MN 55455

HaeOk Skarda Lee
NASA Lewis Research Center,
Cleveland, OH 44135

A flux formulation for a planar slab of molecular gas radiation bounded by diffuse reflecting walls is developed. While this formulation is limited to the planar geometry, it is useful for studying approximations necessary in modeling nongray radiative heat transfer. The governing equations are derived by considering the history of multiple reflections between the walls. Accurate solutions are obtained by explicitly accounting for a finite number of reflections and approximating the spectral effects of the remaining reflections. Four approximate methods are presented and compared using a single absorption band of H_2O. All four methods reduce to an identical zeroth-order formulation, which accounts for all reflections approximately but does handle nonreflected radiation correctly. A single absorption band of CO_2 is also considered using the best-behaved approximation for higher orders. A zeroth-order formulation is sufficient to predict the radiative transfer accurately for many cases considered. For highly reflecting walls, higher order solutions are necessary for better accuracy. Including all the important bands of H_2O, the radiative source distributions are also obtained for two different temperature and concentration profiles.

1 Introduction

Many attempts have been made to analyze radiative heat transfer in an enclosure containing a molecular gas with a gray or sum-of-gray gases model. Fictitious gray gas modeling is clearly inappropriate, as pointed out by Nelson (1977) and others cited in his paper. While the sum-of-gray gases approach can give reasonable results, a large effort may be required to get the appropriate absorption properties (Modest, 1991).

The most accurate nongray gas calculations solve the transfer equation on a line-by-line basis, but this is not practical for engineering problems. The narrow- and wide-band models give the gas absorption or transmittance averaged over a more reasonable band width. In using these band models, careful attention must be paid to the spectral characteristics of the quantities involved as well as their products.

Additional complications occur in nongray gas analyses when the enclosure walls are reflecting. This is because reflected radiation is a strong function of wavenumber and cannot be averaged separately from the transmittance. In order to maintain the physics of the problem correctly and still utilize the available band models, a series expansion of the wall radiosity is used in this work.

Edwards (1962), following the work of Bevans and Dunkle (1960), was probably the first to point out this series expansion method. Bevans and Dunkle (1960) introduced the band energy approximation, which assumed constant radiosities over a narrow band, noting that this may not be accurate for the reflected part of the wall radiosity.

Since the time of Edwards' (1962) publication, significant work on this topic has been carried out by Nelson (1977, 1979a, 1979b, 1984, 1986). In these papers, Nelson develops the zone method (Hottel and Sarofim, 1967) for analyzing molecular gas radiation with band absorption models. Essentially a series solution is cast in the form of a closure problem. The series solution is exact; however, the closure solution is only taken to some finite order and is approximate. The direction of Nelson's work has been to develop the method for more general geometries and situations.

Contributed by the Heat Transfer Division for publication in the JOURNAL OF HEAT TRANSFER. Manuscript received by the Heat Transfer Division June 1992; revision received December 1992. Keywords: Radiation. Associate Technical Editor: R. O. Buckius.

In Kim et al. (1991), a discrete ordinates method is formulated for a planar slab of nongray gas between black, plane-parallel walls. This technique is extended by Menart et al. (1993) to handle reflecting walls properly, taking into account the spectral correlations between wall reflected radiation and gas transmittance for nonisothermal media. Computational times increased by orders of magnitude in going from the black to gray wall analysis.

In this work the problem of radiative transfer between infinite parallel walls enclosing a nonisothermal, molecular gas is once again considered. This time a flux method presented by Soufiani et al. (1985) is further expanded to include the wall reflected radiation correctly. Although this flux method is limited to the one-dimensional plane-parallel geometry, the formulation is perhaps easier to understand than the discrete ordinates method. More importantly, the computational requirements are greatly reduced for the flux method, making it possible to run higher order solutions of different approximation methods to study their behavior. Using the discrete ordinates method, it became computationally costly to run higher than a second-order solution.

II Spectrally Averaged Radiative Transfer Expressions

The radiative flux equation for a one-dimensional slab of absorbing-emitting gases on a spectral basis is

$$q_\nu(x) = q_\nu^+(x) - q_\nu^-(x) \tag{1}$$

where

$$q_\nu^+(x) = 2\pi \int_0^1 I_\nu^+(x_0, \mu)\tau_\nu(x_0 \rightarrow x, \mu)\mu d\mu + 2\pi \int_0^1 \int_{x_0}^{x} I_{\nu b}(x^*) \frac{\partial \tau_\nu(x^* \rightarrow x, \mu)}{\partial x^*} \mu dx^* d\mu \tag{2a}$$

and

$$q_\nu^-(x) = 2\pi \int_0^1 I_\nu^-(x_L, -\mu)\tau_\nu(x_L \rightarrow x, -\mu)\mu d\mu + 2\pi \int_0^1 \int_{x}^{x_L} I_{\nu b}(x^*) \frac{\partial \tau_\nu(x^* \rightarrow x, -\mu)}{\partial x^*} \mu dx^* d\mu. \tag{2b}$$

In the above equations, $I^+(x_0, \mu)$ is the outgoing intensity from the wall at x_0, and $I^-(x_L, -\mu)$ is the outgoing intensity from the wall at x_L. The transmittance and its derivative are defined as

$$\tau_\nu(x^* \rightarrow x, \mu) = \exp\left[-\frac{1}{\mu}\int_{x^*}^{x} a_\nu(x^{**})dx^{**}\right] \quad (3a)$$

$$\mu \frac{\partial \tau_\nu(x^* \rightarrow x, \mu)}{\partial x^*} = a_\nu(x^*)\tau_\nu(x^* \rightarrow x, \mu) \quad (3b)$$

where x_0, x_L, and $-\mu$ can be inserted to get other transmittances and derivatives. The first terms on the right-hand sides of Eqs. (2*a*) and (2*b*) represent the flux from the appropriate wall that is transmitted to position x, and the second terms represent the gas emission contributions to the flux at position x. From this point, the presented derivation will be limited to the positive-directed flux. The derivation is similar for the negative-directed flux.

For this work the narrowband approximation is utilized in the following form:

$$\frac{1}{\Delta\nu}\int_{\Delta\nu} I_{\nu b}\tau_\nu d\nu \approx \bar{I}_{\nu b}\left[\frac{1}{\Delta\nu}\int_{\Delta\nu}\tau_\nu d\nu\right] = \bar{I}_{\nu b}\bar{\tau}_\nu \quad (4)$$

where $\Delta\nu$ is the width of a narrow band, $\bar{I}_{\nu b}$ is the Planck function evaluated at the center wavenumber in $\Delta\nu$, $\bar{\tau}_\nu$ is obtained from the statistical narrowband model with exponential-tailed-inverse line-strength distribution (Malkmus, 1967)

$$\bar{\tau}_\nu(x^* \rightarrow x, \mu) = \exp\left[-\frac{\beta_{\nu,\,\mathrm{eff}}}{\pi}\left(\sqrt{1+\frac{2\pi u(x^*, x, \mu, P)k_{\nu,\,\mathrm{eff}}}{\beta_{\nu,\,\mathrm{eff}}}}-1\right)\right]. \quad (5)$$

The narrowband parameters are taken from Hartmann et al. (1984) and Soufiani et al. (1985). These parameters came from line-by-line calculations and are given in a tabular form for bandwidths of 25 or 50 cm^{-1}. Nonisothermal and inhomogeneous media are treated using the Curtis–Godson method (Godson, 1953; Young, 1977).

Using the narrowband approximation, the wavenumber averaged form of Eq. (2*a*) is written as

$$\bar{q}_\nu^+(x) = 2\pi\int_0^1 \overline{I_\nu^+(x_0, \mu)\tau_\nu(x_0 \rightarrow x, \mu)}\mu d\mu + 2\pi\int_0^1\int_{x_0}^{x}\bar{I}_{\nu b}(x^*)\frac{\partial\bar{\tau}_\nu(x^* \rightarrow x, \mu)}{\partial x^*}\mu dx^* d\mu. \quad (6)$$

For reflecting walls, $I_\nu^+(x_0, \mu)$ and $\tau_\nu(x_0 \rightarrow x, \mu)$ cannot be averaged separately as was done for black walls (Kim et al., 1991). The directly emitted portion of $I_\nu^+(x_0, \mu)$ from the wall can be averaged separately but not the reflected component with its strong wavenumber dependence. Blackbody intensities can be taken out of the wavenumber averaging, because $I_{b\nu}$ is almost a constant over a narrow band.

In order to average the first term on the right-hand side of Eq. (6) properly the wall intensity needs to be expanded into its series expansion, which tracks emitted radiant energy through all wall reflections. This allows the wall radiosity to be expressed in terms of blackbody emission functions and transmittances. It is then possible to apply the narrowband approximation as shown in Eq. (4). A compact, shorthand flux expression can be written for diffuse reflections at the walls using slab-transmittance function, $\bar{T}_\nu^+$;

$$\bar{q}_\nu^+(x) = \pi\left[\bar{\epsilon}_{\nu 0}\bar{I}_{\nu b0}\bar{T}_\nu^+(x_0 \rightarrow x) + \int_{x_0}^{x}\bar{I}_{\nu b}(x^*)\frac{\partial\bar{T}_\nu^+(x^* \rightarrow x)}{\partial x^*}dx^*\right] + \sum_{n=1,3,5\ldots}^{\infty}\left[\pi\bar{\rho}_{\nu 0}^{(n+1)/2}\,\bar{\rho}_{\nu L}^{(n-1)/2}\left\{\bar{\epsilon}_{\nu L}\bar{I}_{\nu bL}\bar{T}_\nu^+(x_L \rightarrow x_w^n \rightarrow x) + \int_{x_L}^{x_0}\bar{I}_{\nu b}(x^*)\frac{\partial\bar{T}_\nu^+(x^* \rightarrow x_w^n \rightarrow x)}{\partial x^*}dx^*\right\}\right] + \sum_{n=2,4,6\ldots}^{\infty}\left[\pi\bar{\rho}_{\nu 0}^{n/2}\,\bar{\rho}_{\nu L}^{n/2}\left\{\bar{\epsilon}_{\nu 0}\bar{I}_{\nu b0}\bar{T}_\nu^+(x_0 \rightarrow x_w^n \rightarrow x) + \int_{x_0}^{x_L}\bar{I}_{\nu b}(x^*)\frac{\partial\bar{T}_\nu^+(x^* \rightarrow x_w^n \rightarrow x)}{\partial x^*}dx^*\right\}\right]. \quad (7)$$

Here n is the order of the expansion, with the zeroth order represented by the first term on the right-hand side. Menart et al. (1993) demonstrated that low wall-reflectivity problems

Nomenclature

a_ν = spectral absorption coefficient, m^{-1}
$-dq/dx$ = total radiative source term, $\mathrm{kW/m^3}$
I_ν = spectral radiative intensity, $\mathrm{kW/(m^2 \cdot sr \cdot cm^{-1})}$
J = total number of spectral bands
$k_{\nu,\,\mathrm{eff}}$ = effective mean line-intensity to spacing ratio, $\mathrm{cm^{-1}\ atm^{-1}}$
L = thickness of the slab, m
n = order of solution or referring to a specific term of expansion
P = pressure, atm
q = total net radiative heat flux in x direction, $\mathrm{kW/m^2}$
T = slab-transmittance functions
u = pressure-path length parameter, atm•m
x = x coordinate, m
$x^* \rightarrow x$ = path length from x^* to x, m
$\beta_{\nu,\,\mathrm{eff}}$ = effective mean line-width to spacing ratio
$\Delta\nu$ = wavenumber interval, cm^{-1}
ϵ_ν = spectral wall emissivity
μ = direction cosine = $\cos\theta$
ρ_ν = spectral wall reflectivity
τ_ν = spectral transmittance

Superscript

*or** = integration variable or position superscript
$\overline{(\ )}$ = spectral average
$+$ = related to positive directed flux
$-$ = related to negative directed flux
a = approximate additional solution
n = order of solution or referring to a specific term of expansion
$n+a$ = truncated series and additional solution added together

Subscripts

0 = grid point number at $x = x_0$
b = blackbody
extra = leftover radiant flux after $n+1$ reflections
g = gas
i = spatial index in x direction
j = spectral index
k = dummy spatial index
L = wall at $x = x_L$
M = grid point number at $x = x_L$
w = wall
ν = spectral

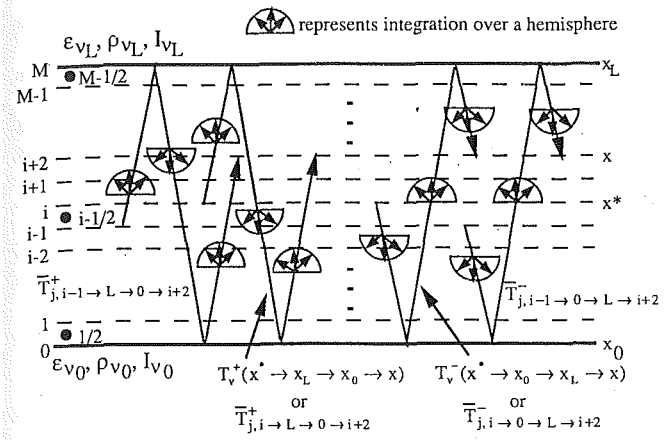

Fig. 1 A schematic of the second-order slab-transmittance functions

can be accurately handled with a zeroth-order closure solution. The quantities $\bar{I}_{vb0}$ and $\bar{I}_{vbL}$ are Planck blackbody emissions at the wall temperatures. Each of the terms in Eq. (7) has the following meaning:

- $n=0$: Radiant energy emitted by the wall at x_0 and the gas between x_0 and x that is directly transmitted to the position x.
- $n=1$: Radiant energy emitted by the wall at x_L and the gas layer that is reflected at x_0 and transmitted to position x.
- $n=2$: Radiant energy emitted by the wall at x_0 and the gas layer that is reflected at x_L and at x_0, and then transmitted to position x.
- $n=n$: Radiant energy emitted by the wall at x_w and the gas layer that is reflected a total of n times and then transmitted to position x.

Zeroth and nth order positive-direction slab-transmittance functions are used in Eq. (7). A *zeroth-order*, positive slab-transmittance function is defined as

$$\overline{T}_v^+(x^*\to x)=2\left(\int_0^1 \tau_v(x^*\to x,\ \mu)\mu d\mu\right), \qquad (8a)$$

where the path from x^* to x is in the positive x direction, or positive μ directions. Higher nth order positive-direction slab-transmittance functions are written in a general form as

$$\overline{T}_v^+(x^*\to x_w^n\to x)=2^{n+1}\cdot\left(\int_0^1 \tau_v(x^*\to x_w,\ \pm\mu)\mu d\mu\right)\left(\int_0^1 \tau_v(x_0\to x_L,\ \mu)\mu d\mu\right)^{n-1}\left(\int_0^1 \tau_v(x_0\to x,\ \mu)\mu d\mu\right), \qquad (8b)$$

where n is the order of the function and indicates the total number of reflections experienced in the path. The term x_w^n represents the n wall locations that are encountered, i.e., . . . $\to x_L \to x_0 \to x_L \to x_0$, with the rightmost parameter always equal to x_0 for positive-directed functions.

The first transmittance integral appearing under the overbar in Eq. (8*b*) is interpreted in the following fashion. The x_w is x_0 when n is odd and x_L for n even. The sign of μ in this transmittance must indicate the direction of the *first* portion of the total path. The derivative of this first transmittance with respect to x^*, multiplied by the rest of the expression under the overbar of Eq. (8*b*), gives the $\partial\overline{T}_v^+/\partial x^*$ terms appearing in Eq. (7). Note that all the factors remain under the overbar.

The positive-direction slab-transmittance functions have the *last* portion of the total path in the positive x direction. The negative slab-transmittance functions are defined in a similar manner, except that the *last* portion of the path is in the negative x direction. For example, the path for a second-order, positive slab-transmittance function from x^* to x is illustrated by the center-left trace shown in Fig. 1 and marked as $T_v^+(x^*\to x_L\to x_0\to x)$. The center-right trace in Fig. 1 illustrates the path for the second-order negative slab-transmittance from $x^*\to x_0\to x_L\to x$ and is marked as $T_v^-(x^*\to x_0\to x_L\to x)$. To indicate that the slab-transmittance functions are an integration of the transmittances over the appropriate hemisphere, the symbol of a half circle with arrows is used. For diffuse walls the integrations must take place for every pass through the gas.

Practically, the spectrally averaged slab-transmittance of Eq. (8*b*) is calculated from Eq. (5) in the following manner:

$$\overline{T}_v^+(x^*\to x_w^n\to x)=2^{n+1}\int_0^1\int_0^1\cdots\int_0^1\exp\left[-\frac{\beta_{v,\,\mathrm{eff}}}{\pi}\cdot\left(\sqrt{1+\frac{2\pi u(x^*,\,x,\,\mu_{n+1},\,\mu_n\ldots\mu_1,\,P)k_{v,\,\mathrm{eff}}}{\beta_{v,\,\mathrm{eff}}}}-1\right)\right]\cdot\mu_{n+1}d\mu_{n+1}\mu_n d\mu_n\ldots\mu_1 d\mu_1 \qquad (9a)$$

where the pressure path length includes the full path under consideration:

$$u(x^*,\,x,\,\mu_{n+1},\,\mu_n\ldots\mu_1,\,P)=P\cdot\left[\left|\frac{x^*-x_{0\text{ or }L}}{\mu_{n+1}}\right|+\left|\frac{x_L-x_0}{\mu_n}\right|+\left|\frac{x_L-x_0}{\mu_{n-1}}\right|+\ldots+\left|\frac{x-x_0}{\ }\right|\right. \qquad (9b)$$

The properties of the spectrally averaged slab-transmittance functions are comparable to those for the spectrally averaged transmittance. It is generally not possible to change the order of the arguments in higher order slab transmittance functions, although $\bar{\tau}_v(x^*\to x,\ \mu)=\bar{\tau}_v(x\to x^*,\ -\mu)$ and $\overline{T}_v^{+\text{or}\,-}(x^*\to x)=\overline{T}_v^{-\text{or}\,+}(x\to x^*)$ for zeroth order. On a spectral basis, $T_v^{+\text{or}\,-}$ can be multiplied and divided to give slab-transmittance functions based on longer or shorter lengths like τ_v. This is not true for spectrally averaged quantities, $\overline{T}_v^{+\text{or}\,-}$ and $\bar{\tau}_v$. That is, multiplication of a $\overline{T}_v^{+\text{or}\,-}$ based on the length L_1 and a $\overline{T}_v^{+\text{or}\,-}$ based on the length L_2 does not give $\overline{T}_v^{+\text{or}\,-}$ for the length L_1+L_2. Also, division of a $\overline{T}_v^{+\text{or}\,-}$ based on L_1+L_2 by a $\overline{T}_v^{+\text{or}\,-}$ based on L_1 gives $\overline{T}_v^{+\text{or}\,-}$ for the last L_2 of the length, not for first L_1. This property will be useful in the development of the approximations in the next section.

Within the limits of the narrowband approximation Eq. (7) and the corresponding equation in the negative direction are correct, but an infinite number of terms must be included for an exact solution. Since the higher order terms decrease in magnitude, a desired level of accuracy may be obtained by including enough terms in the analysis.

III Approximations

In order to decrease the number of terms needed in Eq. (7) for a desired level of accuracy in the radiative flux, methods of approximating the higher order terms in the series solution are considered. Of the many ways to carry out the details of this approximation (Edwards, 1962; Nelson, 1977, 1979b, 1984; Menart et al., 1993), four methods will be discussed here.

The first technique (method I) is the most obvious form of an approximation in that all higher order terms are just neglected, i.e., all terms of order higher than n are ignored in

Eq. (7) for the nth order solution. This approximation will be referred to as the *truncation* solution. The truncation approximation was also considered by Menart et al. (1993) with the discrete ordinates method.

To improve an nth order truncation approximation, the neglected terms in the series expansion must somehow be included. The terms of order higher than n represent the radiant energy that hasn't been absorbed after n complete passes through the gas, not including the emission pass. This leftover energy is called $\bar{q}_{\nu,\,\text{extra}}$, and a gray band assumption is made for this flux. The *additional* fluxes that are due to $\bar{q}_{\nu,\,\text{extra}}$ are found by solving for the resulting flux distribution in absorbing (nonemitting) gas between two diffusely reflecting walls. With boundary fluxes $\bar{q}_{\nu,\,\text{extra}}(x_0)$ and $\bar{q}_{\nu,\,\text{extra}}(x_L)$, a solution is easily obtained as

$$\bar{q}_\nu^{+,a}(x) = [\bar{q}_{\nu,\text{extra}}(x_0) + \bar{\rho}_{\nu 0}\bar{q}_\nu^{-,a}(x_0)]\bar{T}_\nu^{+}(x_0 \to x) \qquad (10a)$$

and

$$\bar{q}_\nu^{-,a}(x) = [\bar{q}_{\nu,\text{extra}}(x_L) + \bar{\rho}_{\nu L}\bar{q}_\nu^{+,a}(x_L)]\bar{T}_\nu^{-}(x_L \to x). \qquad (10b)$$

$\bar{q}_\nu^{+,a}(x)$ and $\bar{q}_\nu^{-,a}(x)$ are the *additional* fluxes that account for the effects of the remaining higher order terms in the series solution in Eq. (7). Equations (10a) and (10b) can be solved simultaneously for $\bar{q}_\nu^{+,a}(x_L)$ and $\bar{q}_\nu^{-,a}(x_0)$ by evaluating Eq. (10a) at x_L and Eq. (10b) at x_0.

The leftover radiant fluxes that haven't been absorbed after n passes through the gas and $n+1$ reflections from the walls are determined from

$$\bar{q}_{\nu,\text{extra}}(x_0) = \bar{\rho}_{\nu 0}[\bar{q}_\nu^{-,n}(x_0) - \bar{q}_\nu^{-,n-1}(x_0)] \qquad (11a)$$

and

$$\bar{q}_{\nu,\,\text{extra}}(x_L) = \bar{\rho}_{\nu L}[\bar{q}_\nu^{+,n}(x_L) - \bar{q}_\nu^{+,n-1}(x_L)] \qquad (11b)$$

where $\bar{q}_\nu^{+,n}(x)$ and $\bar{q}_\nu^{-,n}(x)$ are the nth order series solutions, Eq. (7) including terms 1 through n, and $\bar{q}_\nu^{+,n-1}(x)$ and $\bar{q}_\nu^{-,n-1}(x)$ are the $(n-1)$th series solutions.

The final flux distribution is a sum of the nth order series solution and the corresponding additional flux solution:

$$\bar{q}_\nu^{+,n+a}(x) = \bar{q}_\nu^{+,n}(x) + \bar{q}_\nu^{+,a}(x) \qquad (12a)$$

and

$$\bar{q}_\nu^{-,n+a}(x) = \bar{q}_\nu^{-,n}(x) + \bar{q}_\nu^{-,a}(x). \qquad (12b)$$

The fluxes $\bar{q}_\nu^{+,n+a}(x)$ and $\bar{q}_\nu^{-,n+a}(x)$ approximate the exact $\bar{q}_\nu^{+}(x)$ and $\bar{q}_\nu^{-}(x)$ obtained from Eq. (7). Equations (10), (11), and (12) used with a truncated Eq. (7) is approximation method II.

Approximation method III is obtained by noting that an improvement in Eq. (10) can be made by using higher order band transmittance functions. Nelson (1979b) points out that as the radiant energy travels a longer path length through the gas, a greater fraction of the remaining energy resides in the band wings. Transmission of radiant energy for the last part of the journey should therefore be higher than that for the first part. An expression comparing the transmittances for each successive pass of the radiant energy through the gas can be written by dividing the nth transmittance by the $(n-1)$th transmittance to get the transmittance for just the nth pass;

$$0 < \bar{\tau}_\nu(x_0 \to x_L) < \frac{\bar{\tau}_\nu(x_L \to x_0 \to x_L)}{\bar{\tau}_\nu(x_L \to x_0)} < \frac{\bar{\tau}_\nu(x_0 \to x_L \to x_0 \to x_L)}{\bar{\tau}_\nu(x_0 \to x_L \to x_0)}$$
$$< \frac{\bar{\tau}_\nu(x_L \to x_w^n \to x_L)}{\bar{\tau}_\nu(x_L \to x_w^{n-1} \to x_0)} < \cdots\cdots\cdots$$
$$< \frac{\bar{\tau}_\nu(x_L \to x_w^\infty \to x_L)}{\bar{\tau}_\nu(x_L \to x_w^{\infty-1} \to x_0)} \le 1.0. \qquad (13)$$

A value of one is approached in Eq. (13) if no restrictions are put on the wavenumber limits, while some number less than one is approached with finite wavenumber limits of a narrowband. Since Eq. (13) holds for any μ direction or an integration over all μ's, this same trend holds for the slab transmittance functions.

The third approximation (method III) uses the highest order slab-transmittance function available from the series solution rather than the *zeroth-order* slab-transmission function used in Eq. (10). The following expressions for the additional fluxes are then obtained:

$$\bar{q}_\nu^{+,a}(x) = [\bar{q}_{\nu,\,\text{extra}}(x_0) + \bar{\rho}_{\nu 0}\bar{q}_\nu^{-,a}(x_0)]\frac{\bar{T}_\nu^{+}(x_w \to x_w^n \to x)}{\bar{T}_\nu^{-}(x_w \to x_w^{n-1} \to x_0)} \qquad (14a)$$

and

$$\bar{q}_\nu^{-,a}(x) = [\bar{q}_{\nu,\,\text{extra}}(x_L) + \bar{\rho}_{\nu L}\bar{q}_\nu^{+,a}(x_L)]\frac{\bar{T}_\nu^{-}(x_w \to x_w^n \to x)}{\bar{T}_\nu^{+}(x_w \to x_w^{n-1} \to x_L)}. \qquad (14b)$$

For $n = 0$, methods II and III are equivalent. Note that $\bar{T}_\nu^{+\text{or}-}(x_w \to x_w^n \to x)$ simply takes on the value of one for n less than zero. This third approximation technique is essentially that used by Nelson (1979b) to consider a two-zone enclosure. Eqs. (11), (12), and (14) used with a truncated Eq. (7) is approximation method III.

The last approximation technique to be considered (method IV) is one used by Menart et al. (1993), where this method was developed on an intensity basis for the discrete ordinates formulation. Integrating the governing equations of Menart et al. (1993) over angles gives the required flux representations.

For n odd,

$$\frac{d\bar{q}_\nu^{+,n+a}(x)}{dx} = \frac{d\bar{q}_\nu^{+,n}(x)}{dx} + \bar{\rho}_{\nu 0}^{(n+1)/2}\,\bar{\rho}_{\nu L}^{(n+1)/2}\,\bar{q}_\nu^{+,n+a}(x_L)\,\frac{d\bar{T}_\nu^{+}(x_L \to x_w^n \to x)}{dx} \qquad (15a)$$

and

$$\frac{d\bar{q}_\nu^{-,n+a}(x)}{dx} = \frac{d\bar{q}_\nu^{-,n}(x)}{dx} + \bar{\rho}_{\nu 0}^{(n+1)/2}\,\bar{\rho}_{\nu L}^{(n+1)/2}\,\bar{q}_\nu^{-,n+a}(x_0)\,\frac{d\bar{T}_\nu^{-}(x_0 \to x_w^n \to x)}{dx}. \qquad (15b)$$

For n even,

$$\frac{d\bar{q}_\nu^{+,n+a}(x)}{dx} = \frac{d\bar{q}_\nu^{+,n}(x)}{dx} + \bar{\rho}_{\nu 0}^{(n/2+1)}\,\bar{\rho}_{\nu L}^{n/2}\,\bar{q}_\nu^{-,n+a}(x_0)\,\frac{d\bar{T}_\nu^{+}(x_0 \to x_w^n \to x)}{dx} \qquad (15c)$$

and

$$\frac{d\bar{q}_\nu^{-,n+a}(x)}{dx} = \frac{d\bar{q}_\nu^{-,n}(x)}{dx} + \bar{\rho}_{\nu 0}^{n/2}\,\bar{\rho}_{\nu L}^{(n/2+1)}\,\bar{q}_\nu^{+,n+a}(x_L)\,\frac{d\bar{T}_\nu^{-}(x_0 \to x_w^n \to x)}{dx}. \qquad (15d)$$

For all n the boundary conditions are

$$\bar{q}_\nu^{+,n+a}(x_0) = \bar{\rho}_{\nu 0}\bar{q}_\nu^{-,n+a}(x_0) + \pi\bar{\epsilon}_{\nu 0}\bar{I}_{\nu b0} \qquad (15e)$$

and

$$\bar{q}_\nu^{-,n+a}(x_L) = \bar{\rho}_{\nu L}\bar{q}_\nu^{+,n+a}(x_L) + \pi\bar{\epsilon}_{\nu L}\bar{I}_{\nu bL}. \qquad (15f)$$

In the differential Eqs. (15a)-(15d) the entire fluxes ($\bar{q}_\nu^{n+a}$) are being determined, not just the additional portions as in Eqs. (10) and (14). The first terms on the right-hand sides of Eqs. (15a)-(15d) are series expansion portions, and the second terms are additional portions. In Eqs. (15a)-(15d) the highest order transmittances available are used, but the radiosities in the second terms on the right-hand sides of the equations imply the use of all orders of wall fluxes to obtain a value for the additional flux. While it is not immediately obvious,

Eq. (15) reduces to the sum of the series solutions and the additional flux solutions from Eq. (10) for $n = 0$.

All approximation methods presented above, except the truncation method, give exact results for the gray gas analysis. This is because the only approximation in methods II, III, and IV is that of neglecting correlation effects in obtaining the additional fluxes by assuming gray-bands. The differences in the three methods are in how closely each method approximates the spectral nature of the flux represented by the truncated terms of the series expansion.

IV Discretized Equations

In order to solve Eq. (7) and the corresponding negative-flux equation, a numerical technique is required. Equation (7) in discretized form is

$$\bar{q}^{+}_{j,i} = \pi\left[\bar{\epsilon}_{j0}\bar{I}_{jb0}\bar{T}^{+}_{j,0\to i} + \sum_{k=0}^{i-1}\bar{I}_{jb,k+1/2}(\bar{T}^{+}_{j,k+1\to i} - \bar{T}^{+}_{j,k\to i})\right] + \sum_{n=1,3,5\ldots}^{\infty}\pi\bar{\rho}^{(n+1)/2}_{j0}\,\bar{\rho}^{(n-1)/2}_{jL} \cdot \left\{\begin{array}{l}\bar{\epsilon}_{jL}\bar{I}_{jbL}\bar{T}^{+}_{j,M\to w^n\to i} \\ + \sum_{k=0}^{M-1}\bar{I}_{jb,k+1/2}(\bar{T}^{+}_{j,k\to w^n\to i} - \bar{T}^{+}_{j,k+1\to w^n\to i})\end{array}\right\} + \sum_{n=2,4,6\ldots}^{\infty}\pi\bar{\rho}^{n/2}_{j0}\,\bar{\rho}^{n/2}_{jL}\left\{\begin{array}{l}\bar{\epsilon}_{j0}\bar{I}_{jb0}\bar{T}^{+}_{j,0\to w^n\to i} \\ + \sum_{k=0}^{M-1}\bar{I}_{jb,k+1/2}(\bar{T}^{+}_{j,k+1\to w^n\to i} - \bar{T}^{+}_{j,k\to w^n\to i})\end{array}\right\} \tag{16}$$

where the subscripts 0 and M denote wall locations, i and k denote discretized control volume face locations, and $i + 1/2$ and $k + 1/2$ denote control volume center points (see Fig. 1).

In Fig. 1 the two positive-direction slab-transmittance functions required for the $n = 2$ term in Eq. (16) are shown on the left. The difference of these transmittance functions multiplied by $\bar{I}_{jb,i-1/2}$ gives the amount of emitted radiant energy by control volume $i - 1/2$ that reaches the control surface i. The summation signs in Eq. (16) indicate that this type of emission calculation must be included from every control volume. The two negative-direction slab transmittance functions required for the $n = 2$ term of the $\bar{q}^{-}_{j}$ flux are shown on the right of Fig. 1.

Equation (14) in discretized form is

$$\bar{q}^{+,a}_{j,i} = [\bar{q}_{j,\text{extra},0} + \bar{\rho}_{j0}\bar{q}^{-,a}_{j,0}]\,\frac{\bar{T}^{+}_{j,w\to w^n\to i}}{\bar{T}^{-}_{j,w\to w^{n-1}\to 0}} \tag{17a}$$

and

$$\bar{q}^{-,a}_{j,i} = [\bar{q}_{j,\text{extra},L} + \bar{\rho}_{jL}\bar{q}^{+,a}_{j,M}]\,\frac{\bar{T}^{-}_{j,w\to w^n\to i}}{\bar{T}^{+}_{j,w\to w^{n-1}\to M}}. \tag{17b}$$

Positive and negative directed fluxes can then be obtained from Eq. (12). The $n + a$ superscript on the fluxes will be dropped for the rest of the paper.

The entire $n + a$ flux at any location x (or index i) is

$$q_i = \sum_{j=1}^{J}(\bar{q}^{+}_{j,i} - \bar{q}^{-}_{j,i})\Delta\nu_j \tag{18}$$

and the total radiative source term is found from

Table 1 Comparisons of the four approximate methods for $\rho_w = 0.5$ (3755 cm^{-1} H_2O band, $T_g = 1000$ K, $T_w = 500$ K)

L (m)	Order	Magnitude of Wall Flux (kW/m^2)				Slab Centerline Radiative Source Term (kW/m^3)			
		I	II	III	IV	I	II	III	IV
0.01	0	0.77871	0.69111	0.69111	0.69111	−153.49	−136.28	−136.28	−136.28
	1	0.69798	0.66441	0.66744	0.66582	−137.85	−131.26	−131.82	−131.50
	2	0.67084	0.65738	0.65948	0.65812	−132.55	−129.90	−130.29	−130.02
	3	0.66103	0.65547	0.65662	0.65580	−130.62	−129.52	−129.74	−129.58
	4	0.65732	0.65497	0.65555	0.65511	−129.88	−129.42	−129.53	−129.44
	5	0.65586	0.65485	0.65514	0.65492	−129.59	−129.40	−129.45	−129.41
0.1	0	3.8340	2.5751	2.5751	2.5751	−64.833	−44.122	−44.122	−44.122
	1	2.6821	2.4646	2.4948	2.4737	−46.844	−43.156	−43.367	−42.978
	2	2.5223	2.4663	2.4785	2.4689	−43.947	−42.979	−43.108	−42.926
	3	2.4864	2.4695	2.4740	2.4703	−43.270	−42.973	−43.030	−42.957
	4	2.4765	2.4709	2.4726	2.4712	−43.080	−42.980	−43.004	−42.976
	5	2.4735	2.4715	2.4721	2.4716	−43.021	−42.985	−42.995	−42.984
1.0	0	8.4884	4.8259	4.8259	4.8259	−7.9946	−5.0092	−5.0092	−5.0092
	1	4.9117	4.7163	4.7414	4.7241	−5.2378	−4.9410	−4.9353	−4.9043
	2	4.7586	4.7124	4.7229	4.7152	−4.9721	−4.8932	−4.9042	−4.8895
	3	4.7278	4.7134	4.7177	4.7145	−4.9145	−4.8887	−4.8948	−4.8884
	4	4.7194	4.7143	4.7161	4.7147	−4.8982	−4.8890	−4.8918	−4.8890
	5	4.7167	4.7148	4.7156	4.7150	−4.8930	−4.8895	−4.8907	−4.8896

Table 2 Comparisons of the four approximate methods for $\rho_w = 0.9$ (3755 cm^{-1} H_2O band, $T_g = 1000$ K, $T_w = 500$ K)

L (m)	Order	Magnitude of Wall Flux (kW/m^2)				Slab Centerline Radiative Source Term (kW/m^3)			
		I	II	III	IV	I	II	III	IV
0.01	0	0.78037	0.38684	0.38684	0.38684	−153.81	−76.421	−76.421	−76.421
	1	0.63628	0.36208	0.37466	0.37315	−125.92	−71.952	−74.199	−73.899
	2	0.54925	0.34989	0.36645	0.36341	−108.90	−69.637	−72.655	−72.052
	3	0.49276	0.34364	0.36069	0.35654	−97.787	−68.407	−71.554	−70.730
	4	0.45429	0.34046	0.35653	0.35174	−90.194	−67.756	−70.750	−69.798
	5	0.42720	0.33892	0.35346	0.34842	−84.832	−67.425	−70.152	−69.149
0.1	0	3.8426	0.82853	0.82853	0.82853	−64.981	−14.688	−14.688	−14.688
	1	1.7726	0.76741	0.81023	0.80102	−32.666	−15.295	−14.685	−14.515
	2	1.2569	0.76357	0.80040	0.78805	−23.319	−14.603	−14.547	−14.312
	3	1.0488	0.76532	0.79417	0.78216	−19.397	−14.302	−14.441	−14.208
	4	0.94601	0.76742	0.78989	0.77939	−17.424	−14.169	−14.362	−14.157
	5	0.88887	0.76914	0.78680	0.77797	−16.315	−14.107	−14.304	−14.130
1.0	0	8.5102	1.2257	1.2257	1.2257	−8.0188	−1.4787	−1.4787	−1.4787
	1	2.0767	1.1562	1.2018	1.1926	−3.0652	−1.5743	−1.4717	−1.4549
	2	1.5829	1.1462	1.1895	1.1778	−2.2088	−1.4354	−1.4529	−1.4304
	3	1.4053	1.1456	1.1822	1.1700	−1.8759	−1.4015	−1.4402	−1.4164
	4	1.3176	1.1475	1.1775	1.1659	−1.7072	−1.3920	−1.4317	−1.4088
	5	1.2677	1.1500	1.1744	1.1638	−1.6101	−1.3902	−1.4258	−1.4050

$$-\left(\frac{\partial q}{\partial x}\right)_{i+1/2} = -\frac{q_{i+1} - q_i}{x_{i+1} - x_i}. \tag{19}$$

Equations (18) and (19) hold for any order of solution, with or without an approximation, as long as consistent quantities are used.

V Results and Discussion

Gray wall reflectivities, ρ_w, of 0.5 and 0.9 are considered in this study. It is possible to handle wall reflectivities that vary slowly with wavenumber using this method, but that effect is not considered in this paper.

The first temperature profile considered is uniform with the gas at 1000 K and the walls at 500 K. The walls are kept at a finite temperature to include the effects of wall emission in the survey of approximation techniques. For the results in Tables 1 and 2, only the 3755 cm^{-1} (2.7 μm) band of pure H_2O vapor at one atmosphere is considered, using property

Table 3 Wall flux and source term data for CO_2 utilizing methods I and III (3715 cm^{-1} CO_2 band, T_g = 1000 K, T_w = 500 K)

L (m)	Order	Magnitude of Wall Flux (kW/m²)				Slab Centerline Radiative Source Term (kW/m³)			
		$\rho_w = 0.5$		$\rho_w = 0.9$		$\rho_w = 0.5$		$\rho_w = 0.9$	
		I	III	I	III	I	III	I	III
0.01	0	0.41482	0.35867	0.41571	0.18078	−81.145	−70.197	−81.319	−35.455
	1	0.36151	0.34341	0.32036	0.17398	−70.956	−67.395	−63.099	−34.276
	2	0.34508	0.33869	0.26754	0.16966	−67.765	−66.501	−52.844	−33.486
	3	0.33947	0.33709	0.23517	0.16676	−66.667	−66.194	−46.505	−32.941
	4	0.33744	0.33651	0.21405	0.16474	−66.266	−66.082	−42.348	−32.554
	5	0.33667	0.33630	0.19965	0.16329	−66.114	−66.040	−39.506	−32.274
0.1	0	1.7915	1.1360	1.7954	0.3147	−28.518	−18.291	−28.581	−5.2096
	1	1.1835	1.1015	0.7022	0.3083	−19.588	−18.087	−12.529	−5.2819
	2	1.1129	1.0954	0.4741	0.3053	−18.329	−17.997	−8.4613	−5.2496
	3	1.0985	1.0939	0.3903	0.3036	−18.060	−17.972	−6.8983	−5.2234
	4	1.0948	1.0935	0.3520	0.3026	−17.990	−17.964	−6.1692	−5.2048
	5	1.0937	1.0933	0.3322	0.3019	−17.970	−17.961	−5.7862	−5.1916
1.0	0	3.2400	1.7281	3.2473	0.3985	−2.1700	−1.2588	−2.1752	−0.3464
	1	1.7484	1.7115	0.5631	0.3933	−1.3185	−1.2560	−0.6436	−0.3482
	2	1.7146	1.7083	0.4537	0.3906	−1.2627	−1.2511	−0.4635	−0.3440
	3	1.7091	1.7075	0.4218	0.3889	−1.2526	−1.2496	−0.4049	−0.3411
	4	1.7077	1.7072	0.4076	0.3879	−1.2500	−1.2491	−0.3778	−0.3391
	5	1.7073	1.7072	0.3999	0.3871	−1.2492	−1.2489	−0.3629	−0.3376

data from Hartmann et al. (1984) in the range 2875 cm^{-1} to 4250 cm^{-1}. Table 3 shows results for the 3715 cm^{-1} (2.7 μm) band of pure CO_2 at one atmosphere, using data from Soufiani et al. (1985) in the range 3275 cm^{-1} to 3875 cm^{-1}.

A survey of approximate methods for the one H_2O band is shown in Table 1 for $\rho_w = 0.5$ and in Table 2 for $\rho_w = 0.9$. The wall flux magnitudes and the centerline radiative source terms using four methods discussed in the "Approximations" section are shown in the tables.

In the numerical analysis, nine evenly spaced μ directions were used in a hemisphere to perform angular integrations for slab-transmittance functions. Increasing the number of directions with Simpsons's Rule showed that the integrations converge to three significant digits with nine directions. The data in the tables are shown to five digits. Even though the last two digits have no meaning on an absolute basis, they are helpful for comparing numbers within the two tables. Considering only one absorption band and a small number of angles reduced the computation costs while still allowing for meaningful comparisons between the approximation methods.

The general trend in Table 1 is that methods II, III, and IV show reasonable results even for the zeroth and first orders. Method I lags behind the other techniques in convergence, because higher order terms are simply negelcted in this method. Methods II and IV usually give results that are slightly closer to fifth-order results than method III. The fifth-order results of methods II, III, and IV are the same to three significant figures, and are slightly smaller than the fifth-order method I result. Zeroth-order results for methods II, III, and IV are *identical* and are within 5.4 percent of the fifth-order method I result, and first-order closure results are within 1.8 percent.

All four methods in Table 1 show monotonically decreasing magnitudes toward correct results for each succeeding higher order solution for L = 0.01 m. This behavior is not seen for methods II and IV with larger plate spacings. Although the oscillations are small, this solution behavior is undesirable. A steadily decreasing behavior is desirable so that an assessment of the error in each order of the solution can be made.

Table 2 results for $\rho_w = 0.9$ show slower convergence than Table 1 results for $\rho_w = 0.5$. Method I does not even show the first two digits repeating for the fourth and fifth orders. This is understandable for strongly reflecting walls, since the truncation solution simply neglects higher order reflections. Since fifth-order method III results in Table 1 show best agreement with correct solutions (fifth-order method I), the results from the fifth-order method III approximation will be used here as a convenient standard for comparison. This is not to imply that fifth-order method III solutions are necessarily exact.

In Table 2 as in Table 1, the oscillations in method II wall flux and radiative source-term solutions are present for L = 0.1 and 1.0 m. No oscillations are present for method IV, and method III results are once again well behaved. The first-order wall flux solutions for methods II and IV are closer to the fifth-order results than method III; however, in this case the first-order method II radiative source term can be less accurate than a zeroth-order solution. All zeroth-order approximate solutions are within 9.4 percent of the fifth-order method III result, and within 6.0 percent for first-order solutions.

The results from method III are well behaved because the highest order available slab-transmittances and wall fluxes are used in the analysis, and this best approximates the trends of the neglected terms. In method II the highest order wall flux is used, but the zeroth-order slab-transmittances are used for every order of approximation. As mentioned in the "Approximations" section, the zeroth-order slab-transmittance is smaller than higher order slab-transmittances for the same path length. In method IV highest order transmittances are used, but the wall flux is basically a combination of all orders of terms up to and including order n with the zeroth and first-order terms being dominant. Unlike methods II and IV, method III always uses the best information available on the correlation effects for the required wall fluxes and slab-transmittances. Since method III shows the best characteristics, this approximation will be used in the rest of the results presented.

Table 3 presents the wall flux magnitudes and the centerline radiative source terms for the pure CO_2 gas layer at 1000 K, bounded by diffusely reflecting walls at 500 K. Only the truncation solution (method I) and the best-behaved approximation solution for the H_2O analysis (method III) are compared for ρ_w of 0.5 and 0.9.

The CO_2 results in Table 3 also show that reasonable results are obtained with just a zeroth or first-order method III solution. Method I lags behind method III results in convergence, but higher order solutions are seen to approach limiting final solutions faster for ρ_w = 0.5 than for ρ_w = 0.9. For ρ_w = 0.5, the zeroth-order method III results are within 6.7 percent of the corresponding fifth-order method III results, and the first-order results are within 2.2 percent. For ρ_w = 0.9, the zeroth-order method III results are within 10.8 percent of the corresponding fifth-order method III results, and the first-order results are within 6.6 percent. This is similar to the H_2O results. Method III wall flux results for CO_2 are still well behaved, decreasing toward higher order solutions without any oscillation for all cases considered. Small fluctuations in method III radiative source terms are seen for the highly reflecting ρ_w = 0.9 and L = 0.1 m and 1.0 m.

Finally, H_2O gas layers are considered to show the effects of nonuniform temperature and concentration profiles. For the data presented in Figs. 2–4, all important water absorption bands are considered (rotation band, 6.3, 2.7, 1.87, and 1.38 μm). Results are presented for two temperature profiles in combination with two concentration profiles. The uniform temperature profile used in Tables 1–3 is again used, and a parabolic-like temperature profile described by Kim et al. (1991) is also used. The maximum temperature of this profile is 1111 K, and the wall temperatures are 400 K. A pure, uniform H_2O concentration profile and a parabolic concentration profile (see Kim et al., 1991) are the distributions of the participating species used. The parabolic concentration profile is 100 percent H_2O at the center and 0 percent at the walls. Since the total pressure is always kept at one atmosphere for all the data presented in this paper, the remaining gas in the parabolic

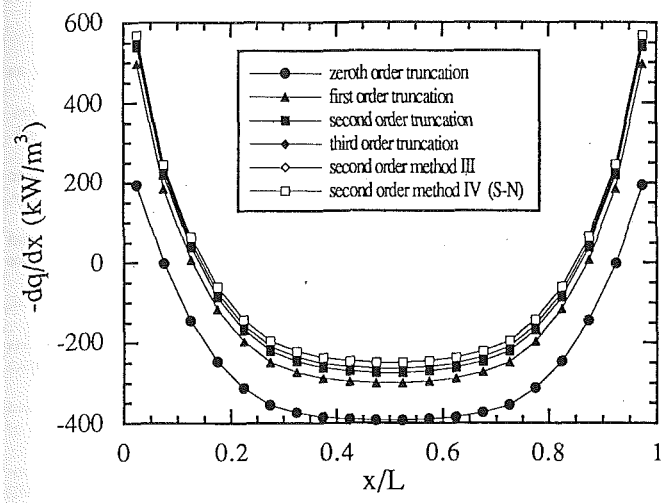

Fig. 2 Radiative source distributions for the parabolic-like temperature profile, uniform H_2O concentration profile, ρ_w = 0.9, and L = 0.1 m

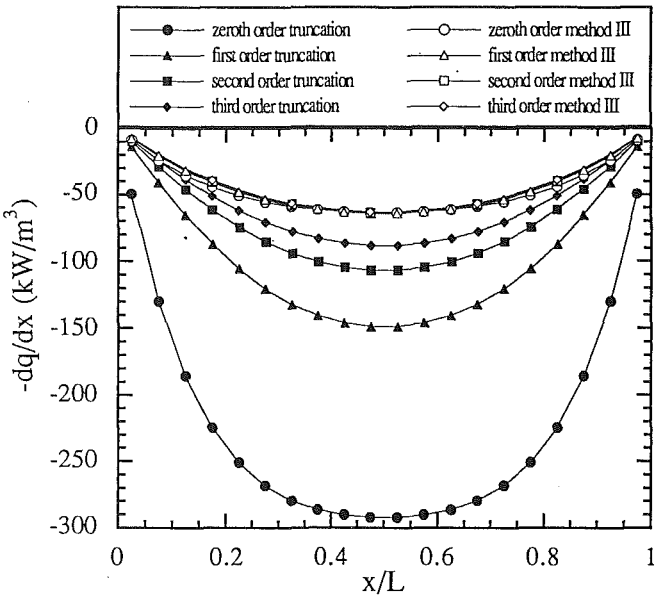

Fig. 3 Radiative source distributions for the uniform gas temperature of 1000 K, parabolic H_2O concentration profile, T_w = 500 K, ρ_w = 0.9, and L = 0.1 m

concentration profile is nitrogen. Nitrogen is a nonparticipating gas, but it affects how H_2O vapor emits and absorbs radiation.

Results for a parabolic-like temperature profile with a pure H_2O concentration are shown in Fig. 2. This case was analyzed using the *S–N* discrete ordinates method by Menart et al. (1993). In Fig. 2 the second-order *S–N* results using approximation method IV are located directly over the second-order flux technique results using method III. While not presented here, excellent agreement has been obtained between the flux and *S–N* solutions for all cases of Menart et al. (1993). For the situation in Fig. 2 the gas is a net emitter everywhere except close to walls. The gas near the walls is a net absorber due to the wall radiation. Note that third-order truncation method solutions lie just below method III results, indicating near convergence.

In Fig. 3 the uniform temperature profile with a parabolic concentration profile is considered. Again up to a third-order solution is shown with practically no difference in method III results. This time, however, the difference between method III results and the third-order truncation solutions is very noticeable. These particular temperature and concentration profiles allow a greater fraction of the radiant energy to survive more than three passes through the absorbing gas media.

Figure 4 presents the combined case of the parabolic type temperature profile (Fig. 2), and the parabolic concentration profile (Fig. 3). The two humps in these radiative source profiles near the walls can be explained as follows. The gas next to radiating walls tends to be a net absorber as was seen in Fig. 2. Furthermore, since the H_2O concentration goes to zero at the walls, the radiative source terms must also go to zero at the walls. This is seen to occur in Fig. 4 as well as Fig. 3. The curves do not go exactly to zero because 20 control volumes were used in this analysis, and the closest gas grid point is located at a small distance from a wall. The hump in the middle is present, because the hot gas in the center portion of the slab is a net emitter in Figs. 2, 3, and 4.

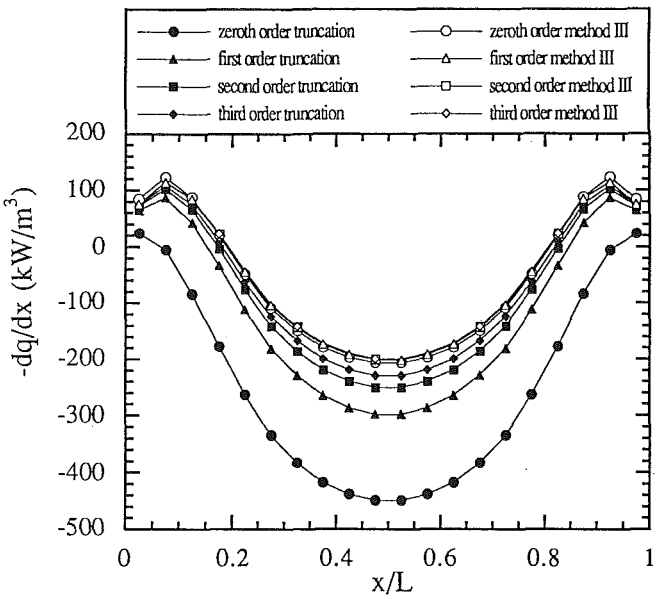

Fig. 4 Radiative source distributions for the parabolic-like temperature profile, parabolic H_2O concentration profile, ρ_w = 0.9, and L = 0.1 m

VI Conclusions

Another method of studying the spectral correlation effects between the wall reflected radiant energy and the transmittance has been developed. This particular technique is restricted to the planar geometry, but the formulation begins with the familiar flux equations for an absorbing, emitting medium. It may thus be easier to understand some of the principles involved in molecular gas radiative heat transfer between reflecting walls utilizing this method as compared to other more advanced techniques.

Furthermore, the flux method requires less computational time than the rigorous discrete ordinates technique for nongray gases. This allows higher order solutions to be calculated at a more reasonable cost. Higher order solutions are needed for comparing approximation techniques. A comparison of Cray-YMP C.P.U. times for the case in Fig. 2 for example, shows that the zeroth-order flux method is more than 30 times faster than a comparable accuracy *S–N* method. The second-order flux method requiring almost 200 s is about 20 times faster than the *S–N* method. The C.P.U. times are a strong function of order of approximation and discretization.

A single H_2O absorption band study showed that approximation methods II, III, and IV all give reasonable results, but

method III is the most well behaved and allows for an assessment of errors at a given order of solution. Methods II and IV show undesirable oscillations as the order of solution is increased. Regardless of the method, higher order solutions are required to obtain good accuracy for high wall-reflectivity problems. For $\rho_w < 0.5$, zeroth-order approximations predict the fluxes and radiative source terms to within 5.4 percent. For $\rho_w = 0.9$, the zeroth-order method III solutions are within 9.4 percent of the fifth-order results. While more accurate results are obtained with higher order solutions, the computer times for higher order solutions increase at an exponential rate while the accuracy increases very slowly. When a single band of CO_2 was studied, there was little difference in the findings from those of the single H_2O band study.

Methods I and III are also used to study nonisothermal and inhomogeneous H_2O layers, including all important absorption bands. Method III approximate solutions for radiation source distributions show little differences between successive orders. The gas concentration and temperature profiles of the slab are shown to have an important effect on the radiative source distributions.

Since the conclusions drawn in this paper are based on the data presented, care should be exercised in extending them to other conditions. The strongest influence on the order of solution required for a desired accuracy appears to be the wall reflectivities, but there are other factors such as wall and gas temperatures, optical depth, type of absorbing species, and concentration profile of the absorbing species. A more extensive study needs to be performed to determine the effects of all of the pertinent parameters for a given application.

Acknowledgments

This work was supported in part by National Science Foundation Grant No. NSF/CTS-8451076 and NASA Grant No. NGT-50830. A grant from the Minnesota Supercomputer Institute is also gratefully acknowledged.

References

Bevans, J. T., and Dunkle, R. V., 1960, "Radiant Interchange Within an Enclosure," ASME JOURNAL OF HEAT TRANSFER, Vol. 82, pp. 1–19.

Edwards, D. K., 1962, "Radiation Interchange in a Nongray Enclosure Containing an Isothermal Carbon-Dioxide–Nitrogen Gas Mixtures," ASME JOURNAL OF HEAT TRANSFER, Vol. 84, pp. 1–11.

Godson, W. L., 1953, "The Evaluation of Infrared Radiation Fluxes Due to Atmospheric Water Vapor," *Quarterly Journal of Royal Meteorological Society*, Vol. 79, pp. 367–379.

Hartmann, J. M., Levi Di Leon, R., and Taine, J., 1984, "Line-by-Line and Narrow-Band Statistical Model Calculations for H_2O," *Journal of Quantitative Spectroscopy and Radiative Transfer*, Vol. 32, No. 2, pp. 119–127.

Hottel, H. C., and Sarofim, A. F., 1967, *Radiative Transfer*, McGraw-Hill, New York.

Kim, T.-K., Menart, J. A., and Lee, H. S., 1991, "Nongray Radiative Gas Analyses Using the *S–N* Discrete Ordinates Method," ASME JOURNAL OF HEAT TRANSFER, Vol. 113, pp. 946–952.

Malkmus, W., 1967, "Random Lorentz Band Model With Exponential-Tailed S^{-1} Line-Intensity Distribution Function," *Journal of the Optical Society of America*, Vol. 57, No. 3, pp. 323–329.

Menart, J. A., Lee, H. S., and Kim, T.-K., 1993, "Discrete Ordinates Solutions of Nongray Radiative Transfer With Diffusely Reflecting Walls," ASME JOURNAL OF HEAT TRANSFER, Vol. 115, pp. 184–193.

Modest, M. F., 1991, "The Weighted-Sum-of-Gray-Gases Model for Arbitrary Solution Methods in Radiative Transfer," ASME JOURNAL OF HEAT TRANSFER, Vol. 113, pp. 650–656.

Nelson, D. A., 1977, "Radiation Heat Transfer in Molecular-Gas Filled Enclosures," ASME Paper No. 77-HT-16.

Nelson, D. A., 1979a, "Band Radiation Within Diffuse-Walled Enclosures: Part I—Exact Solutions for Simple Enclosures," ASME JOURNAL OF HEAT TRANSFER, Vol. 101, pp. 81–84.

Nelson, D. A., 1979b, "Band Radiation Within Diffuse-Walled Enclosures: Part II—An Approximate Method Applied to Simple Enclosures," ASME JOURNAL OF HEAT TRANSFER, Vol. 101, pp. 85–89.

Nelson, D. A., 1984, "Band Radiation of Isothermal Gases Within Diffuse-Walled Enclosures," *International Journal of Heat and Mass Transfer*, Vol. 27, No. 10, pp. 1759–1769.

Nelson, D. A., 1986, "Nongray Total Radiation Within an Enclosure," ASME Paper No. 86-HT-29.

Soufiani, A., Hartmann, J. M., and Taine, J., 1985, "Validity of Band-Model Calculations for CO_2 and H_2O Applied to Radiative Properties and Conductive-Radiative Transfer," *Journal of Quantitative Spectroscopy and Radiative Transfer*, Vol. 33, No. 3, pp. 243–257.

Young, S. J., 1977, "Nonisothermal Band Model Theory," *Journal of Quantitative Spectroscopy and Radiative Transfer*, Vol. 18, pp. 1–28.